Supporting Information for

Photochemically Tuned Magnetic Properties in Er(III)-Based Easy-Plane Single-Molecule Magnet

Jing Li,[†] Ming Kong,[†] Lei Yin,[§] Jing Zhang,[†] Fei Yu,[†] Zhong-Wen Ouyang,[§] Zhenxing Wang,*[,§] Yi-Quan Zhang,*[,‡] and You Song*[,†]

[†]State Key Laboratory of Coordination Chemistry, School of Chemistry and Chemical Engineering, Nanjing University, Nanjing 210023, P. R. China

[‡]Jiangsu Key Laboratory for NSLSCS, School of Physical Science and Technology, Nanjing Normal University, Nanjing 210023, P. R. China

[§]Wuhan National High Magnetic Field Center & School of Physics, Huazhong University of Science and Technology, Wuhan 430074, P. R. China

Corresponding Authors:

* E-mail: yousong@nju.edu.cn

* E-mail: zhangyiquan@njnu.edu.cn

* E-mail: zxwang@hust.edu.cn

Table of contents

1. Structure information

Crystallographic Information. Crystallographic data were collected on Bruker Smart CCD area-detector diffractometer with Mo Kα radiation at 296 K. The diffraction data were treated using SAINT, and SADABS used all absorption corrections. All non-hydrogen atoms were determined by the Patterson method using the SHELXS programs. Hydrogen-bonded were determined theoretically and refined with isotropic thermal parameters riding on their parents. All non-hydrogen atoms were refined by full-matrix least-squares on F2. All calculations were performed by SHELXTL-97.[S1] All non-hydrogen atoms were refined with anisotropic displacement parameters. CCDC 1535027, 1535028, 1873175, and 1873176 contain the supplementary crystallographic data for this paper. These data can be obtained from The Cambridge Crystallographic Data Centre via www.ccdc.cam.ac.uk/data_request/cif.

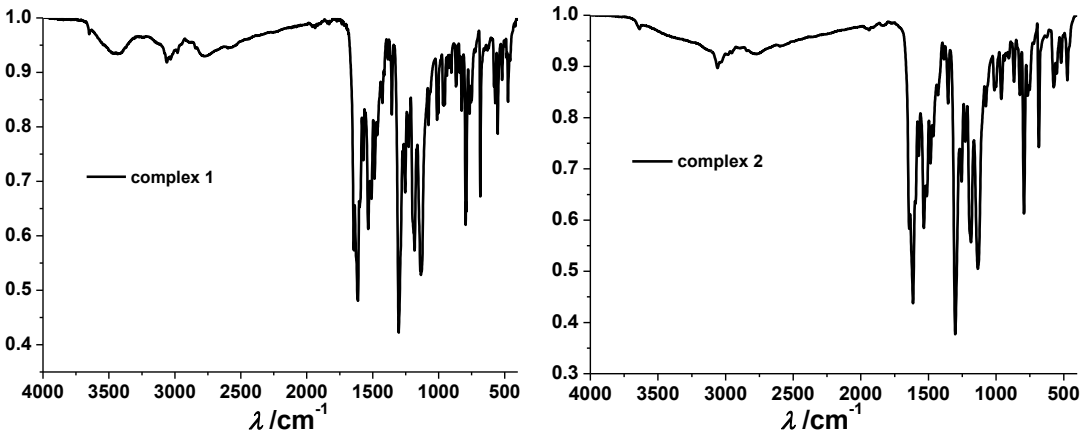

Figure S1. IR of complexes **1**(left) and **2**(right).

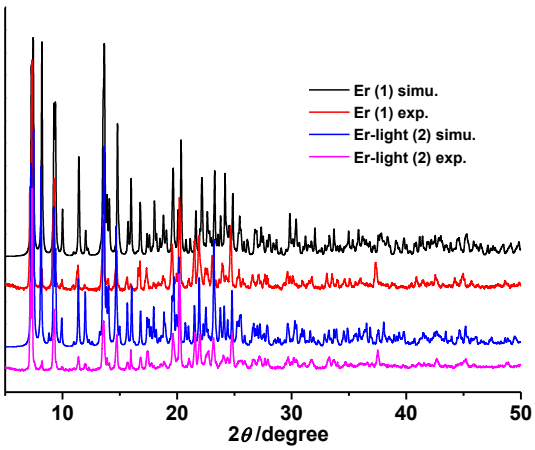

Figure S2. X-ray powder diffraction patterns of complex **1** and **2**.

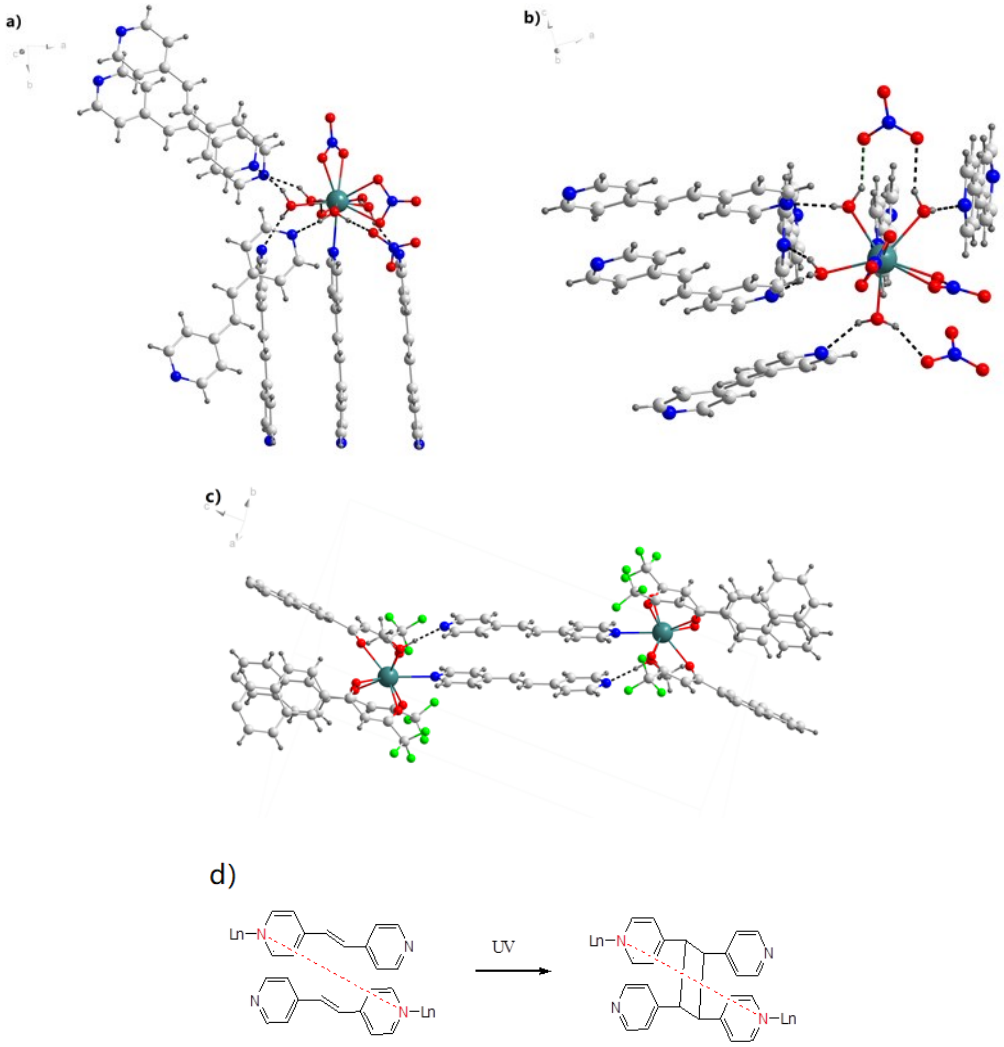

Figure S3. a, b) The intermolecular hydrogen bonds surround the Dy(III) ion in the complex in Liu's work. c) the intramolecular hydrogen bonds in **1**. d) The schematic diagram for the photochemical reaction in dpe dimer in complex **1** and complex in Liu's work. Definition: L(N-N) represents the distance of the red dotted line.

Table S1. Shape measurements of **1**, **2** (the smallest value is shown in RED). We used all the shapes defined in the SHAPE program.[S2] The closer the number is to zero the closer the geometry is to the perfect defined geometry. Code: HBPY - hexagonal bipyramid, SAPR - square antiprism, TDD - triangular dodecahedron, JGBF - Johnson – Gyrobifastigium (J26), JBTPR - Johnson - Biaugmented trigonal prism (J50), BTPR - Biaugmented trigonal prism, JSD - Snub disphenoid (J84).

Complex	**JBTPR**	**BTPR**	**JSD**	**HBPY**	**SAPR**	**TDD**	**JGBF**
1	2.028	1.767	2.641	0.636	1.699	0.532	13.340
2	2.380	2.19	2.468	1.108	2.158	0.397	12.992

Table S2. Crystallographic data for complexes **1**, **2**, **3**, and **4**.

	1	**2**	**3**	**4**
Formula	$C_{55}H_{38}ErF_9N_2O_7$	$C_{110}H_{76}Er_2F_{18}N_4O_{14}$	$C_{55}H_{38}YF_9N_{27}$	$C_{110}H_{76}Y_2F_{18}N_4O_{14}$
Mr [gmol^{-1}]	1177.13	2354.27	1098.78	2197.56
Crystal system	monoclinic	monoclinic	monoclinic	monoclinic
Space group	$P2_1/n$	$P2_1/n$	$P2_1/n$	$P2_1/n$
a [Å]	13.0930(12)	13.2068(14)	13.1386(16)	13.0954(8)
b [Å]	15.4689(14)	15.5253(17)	15.474(2)	15.3301(10)
c [Å]	23.962(2)	23.831(2)	23.964(3)	23.7198(13)
α [º]	90.00	90.00	90.00	90.00
β [º]	98.0260(10)	97.5012(19)	98.178(4)	97.709(2)
γ [º]	90.00	90.00	90.00	90.00
V [Å^3]	4805.67	4844.5(9)	4822.3(1)	4718.8(5)
T [K]	296(2)	296(2)	296(2)	296(2)
Z	4	2	4	2
ρ_{calcd} / g cm^{-3}	1.627	1.614	1.513	1.547
data measured	42818	32794	36350	42011
indep reflns	10981	11175	11083	10956
R_{int}	0.0416	0.1509	0.0916	0.0981
reflns with $I > 2\sigma(I)$	9647	6337	7340	6871
parameter	672	672	669	669
restraints	0	0	0	0
R_1, wR_2	0.0263, 0.0817	0.0563, 0.1081	0.0540, 0.1302	0.0594, 0.1455
GOF	1.104	0.876	0.886	0.949
Largest residuals [e Å^{-3}]	0.6, -0.849	1.261, -1.283	0.374 -0.579	0.945 -0.576
ccdc	1535027	1535028	1873176	1873175

$R_1 = \Sigma||F_0|-|F_c||/\Sigma|F_0|$, $wR_2 = \{\Sigma[w(F_0^2-F_c^2)^2]/\Sigma[w(F_0^2)^2]\}^{1/2}$

2. Magnetization information

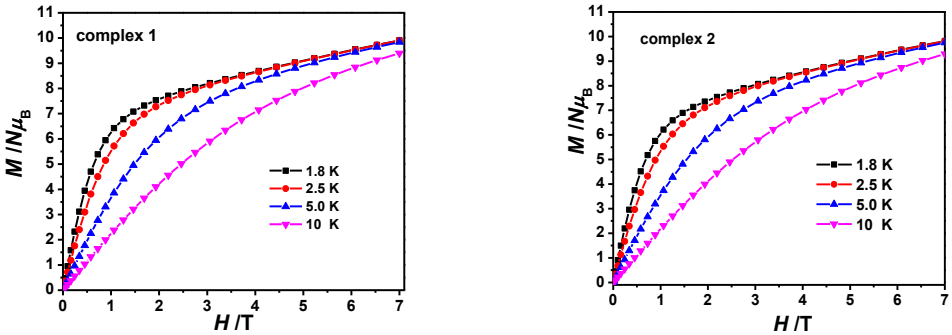

Figure S4. The isothermal field-dependence magnetization of **1** and **2** at low temperature.

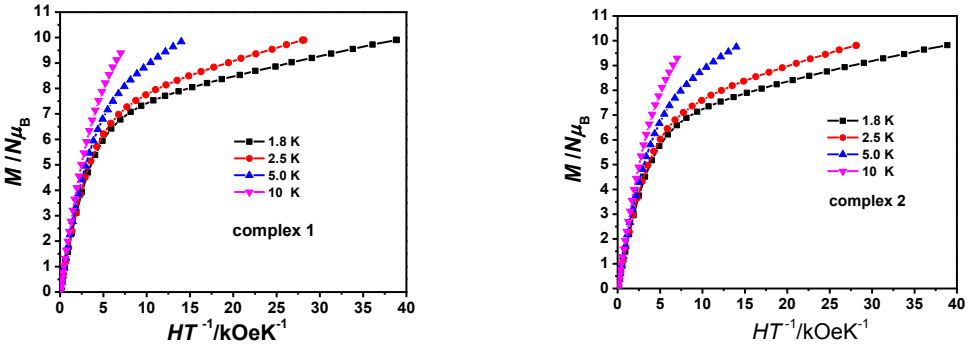

Figure S5. The *M* vs. *H*/*T* data of complex **1** and **2** at 1.8, 2.5, 5, and 10 K.

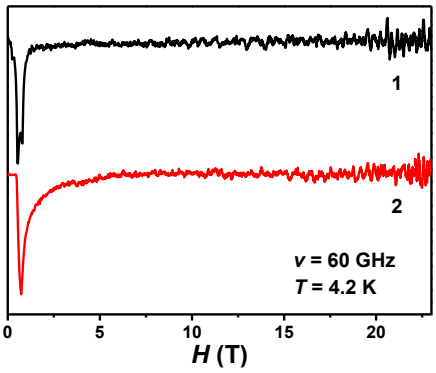

Figure S6 HF-EPR spectrum for a polycrystalline sample of **1**and **2** at 60 GHz and 4.2 K.

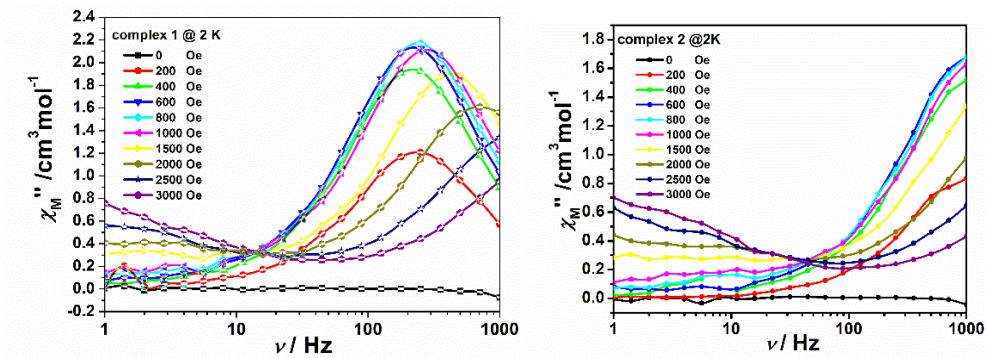

Figure S7. Field dependence *ac* susceptibility of complex **1** (left) and complex **2** (right) at 2 K. At low frequency region, the peak is unclear due to the unstability of VSM equipment.

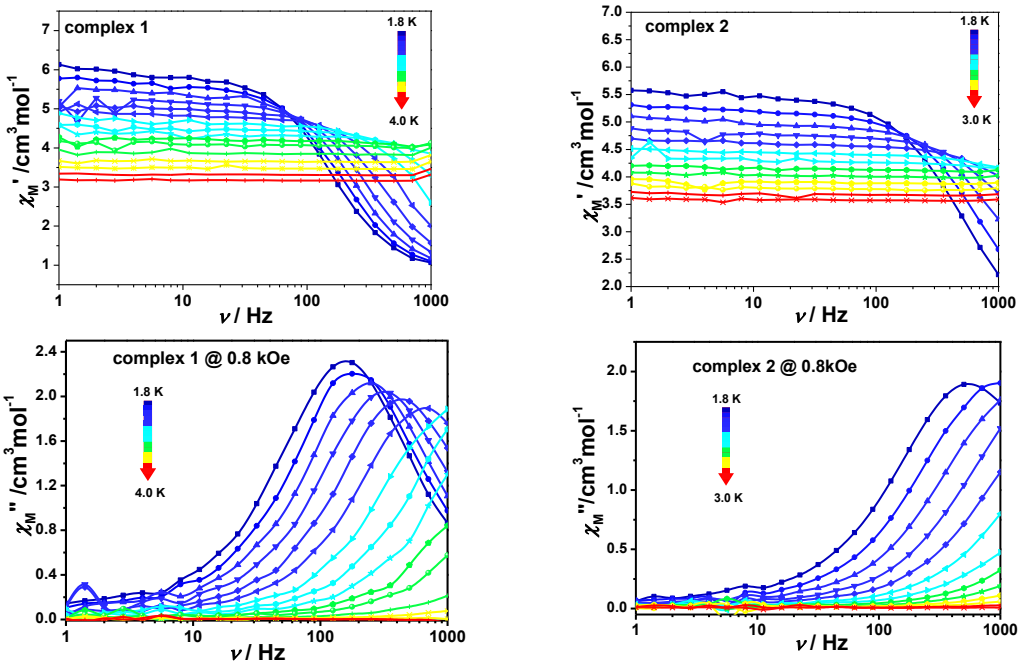

Figure S8. In-phase (χ_M') and out-of-phase (χ_M") ac susceptibilities under 800 Oe dc field (1-999 Hz, by MPMS VSM) at indicated temperatures and frequencies for complex **1** and **2**, respectively

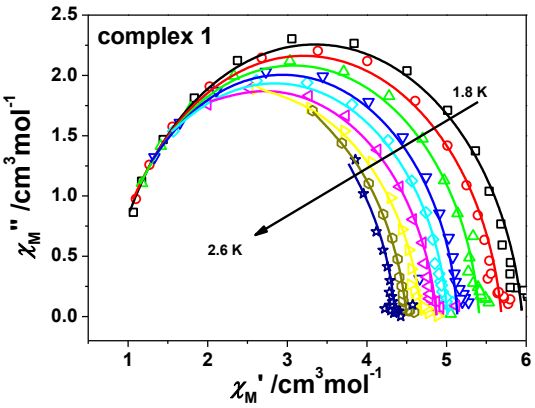

Figure S9. Variable temperature Cole-Cole plots of complex **1** under 800 Oe dc field (1-999 Hz, by MPMS Squid VSM). Fitted parameters are compiled in Supplementary Table S3.

Table S3. Analysis of Cole-Cole plot of complex **1** under 800 Oe dc field

T/ K	χ_S (cm^{3}mol^{-1})	χ_t (cm^{3}mol^{-1})	τ (s)	α	*R*
1.8	7.49E-01	5.95E+00	1.01E-03	8.11E-02	1.40E-01
1.9	7.31E-01	5.69E+00	8.32E-04	7.76E-02	9.53E-02
2	7.49E-01	5.41E+00	6.54E-04	6.21E-02	2.20E-01
2.1	7.51E-01	5.14E+00	4.93E-04	4.63E-02	4.69E-01
2.2	6.77E-01	5.01E+00	3.60E-04	6.27E-02	1.32E-01
2.3	5.61E-01	4.88E+00	2.40E-04	8.19E-02	1.21E-01
2.4	2.95E-01	4.69E+00	1.43E-04	9.51E-02	1.11E-01
2.5	7.21E-06	4.50E+00	8.36E-05	8.57E-02	5.10E-02
2.6	1.25E-05	4.36E+00	5.18E-05	6.93E-02	1.16E-01

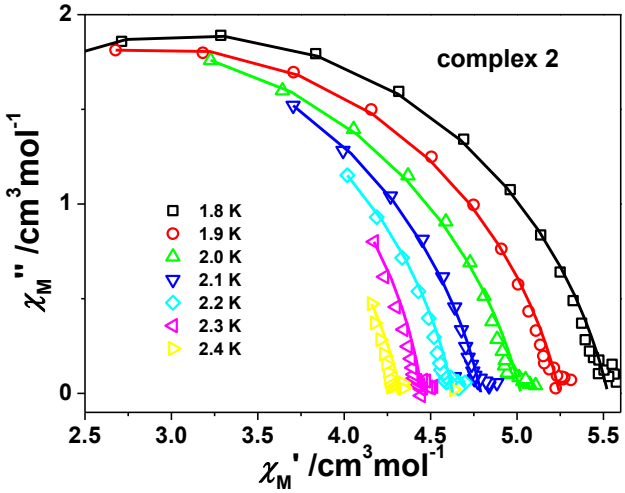

Figure S10. Variable temperature Cole-Cole plots of complex **2** under 800 Oe dc field (1-999 Hz, by MPMS Squid VSM). Fitted parameters are compiled in Supplementary Table S4.

Table S4. Analysis of Cole-Cole plot of complex **2** under 800 Oe dc field

T/ K	χ_S (cm^{3}mol^{-1})	χ_t (cm^{3}mol^{-1})	τ (s)	α	*R*
1.8	6.72E-01	5.53E+00	2.80E-04	1.56E-01	4.34E-02
1.9	5.89E-01	5.25E+00	1.85E-04	1.54E-01	4.08E-02
2	2.28E-01	5.02E+00	1.08E-04	1.69E-01	5.03E-02
2.1	3.64E-15	4.79E+00	6.52E-05	1.47E-01	6.21E-02
2.2	6.04E-15	4.63E+00	4.16E-05	1.32E-01	4.85E-02
2.3	1.14E-14	4.45E+00	2.70E-05	9.14E-02	4.95E-02
2.4	1.31E-14	4.33E+00	1.33E-05	1.46E-01	1.56E-01

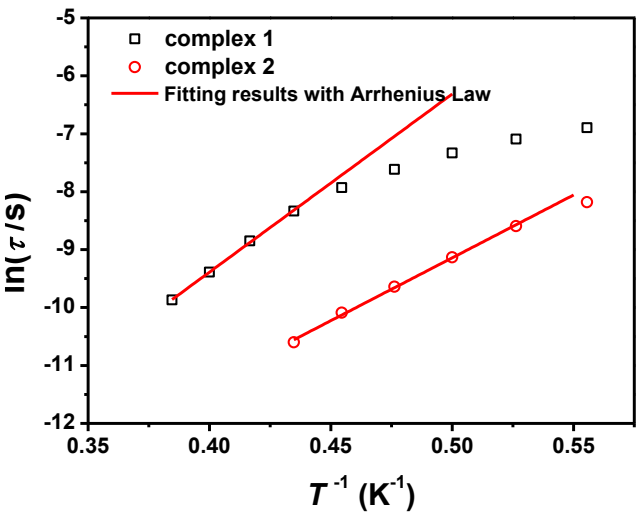

Figure S11 Temperature dependence of ln(τ) extracted from ac susceptibility measurements for complexes **1** and **2** at different temperatures. The solid lines are the fits of Arrhenius Law.

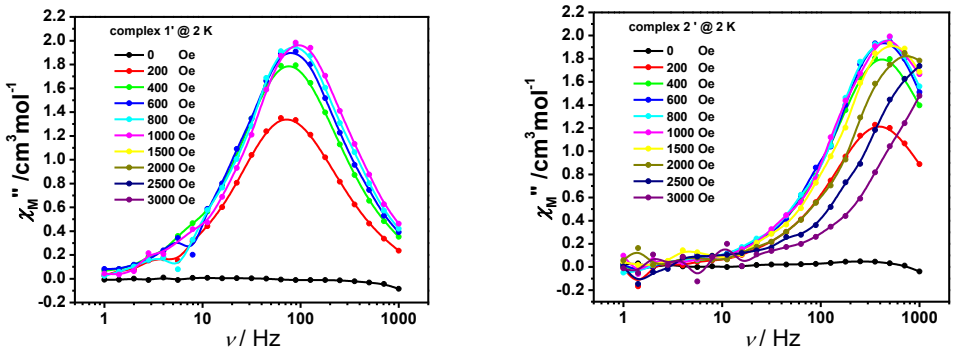

Figure S12. Field dependence *ac* susceptibility of complex **1'** (left) and complex **2'** (right) at 2 K.

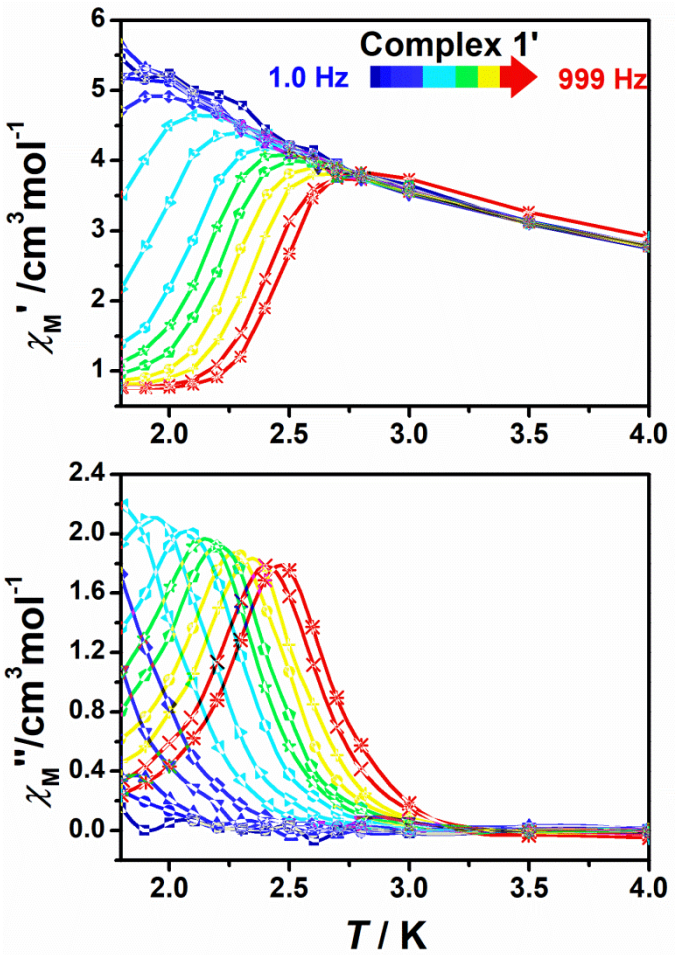

Figure S13. In-phase (χ_M') and out-of-phase (χ_M") ac susceptibilities under 600 Oe dc field (1-999 Hz, by MPMS VSM) at indicated temperatures and frequencies for complex **1'**, respectively.

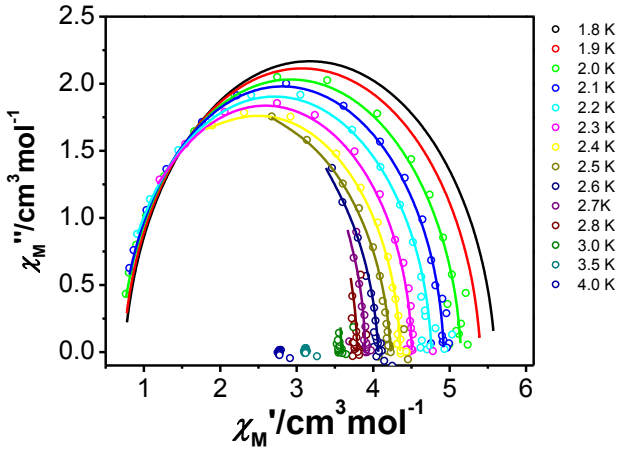

Figure S14. Variable temperature Cole-Cole plots of complex **1'** under 600 Oe dc field (1-999 Hz, by MPMS Squid VSM). Fitted parameters are compiled in Supplementary Table S5.

Table S5. Analysis of Cole-Cole plot of complex **1'** under 600 Oe dc field

T/ K	χ_S (cm^{3}mol^{-1})	χ_t (cm^{3}mol^{-1})	τ (s)	α	*R*
1.8	7.48E-01	5.59E+00	4.20E-03	6.05E-02	4.24E-01
1.9	7.34E-01	5.40E+00	2.95E-03	5.29E-02	3.30E-01
2.0	6.98E-01	5.15E+00	1.91E-03	4.75E-02	9.31E-02
2.1	7.03E-01	4.92E+00	1.19E-03	2.95E-02	9.28E-02
2.2	6.58E-01	4.76E+00	7.25E-04	3.69E-02	1.83E-01
2.3	6.76E-01	4.50E+00	4.25E-04	1.51E-02	1.94E-01
2.4	6.38E-01	4.35E+00	2.40E-04	2.29E-02	8.85E-02
2.5	3.27E-01	4.23E+00	1.26E-04	5.55E-02	1.57E-01
2.6	2.50E-14	4.07E+00	6.40E-05	4.96E-02	1.16E-01
2.7	4.24E-14	3.89E+00	3.96E-05	8.90E-16	1.02E-01
2.8	6.38E-14	3.79E+00	2.37E-05	8.88E-16	7.22E-02
3.0	1.03E-13	3.58E+00	8.24E-06	1.28E-15	1.12E-01
3.5	1.38E-13	3.12E+00	4.17E-20	1.75E-15	5.49E-02
4.0	1.33E-13	2.78E+00	5.84E-20	2.26E-15	6.10E-02

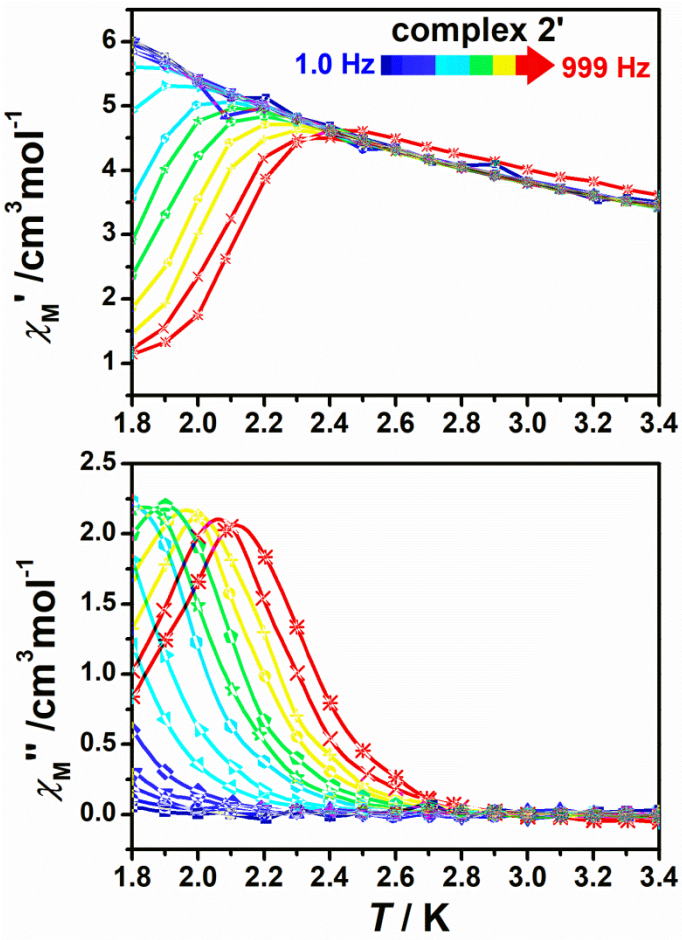

Figure S15. In-phase (χ_M') and out-of-phase (χ_M") ac susceptibilities under 600 Oe dc field (1-999 Hz, by MPMS VSM) at indicated temperatures and frequencies for complex **2'**, respectively.

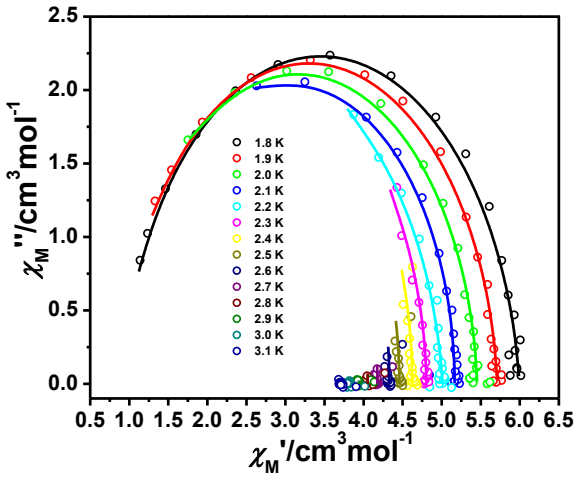

Figure S16. Variable temperature Cole-Cole plots of complex **2'** under 600 Oe dc field (1-999 Hz, by MPMS Squid VSM). Fitted parameters are compiled in Supplementary Table S6.

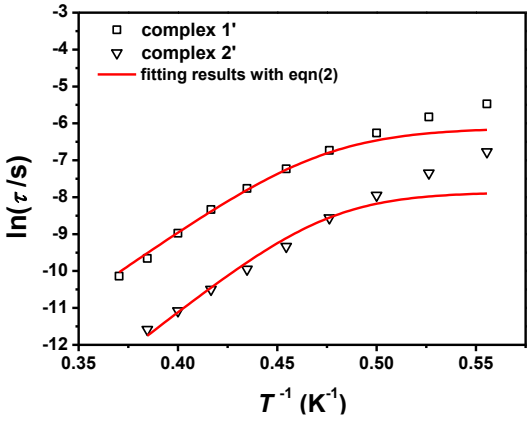

Figure S17 Temperature dependence of ln(τ) extracted from ac susceptibility measurements for complexes **1'** and **2'** at different temperatures. The solid lines are fitting results with eqn (2).

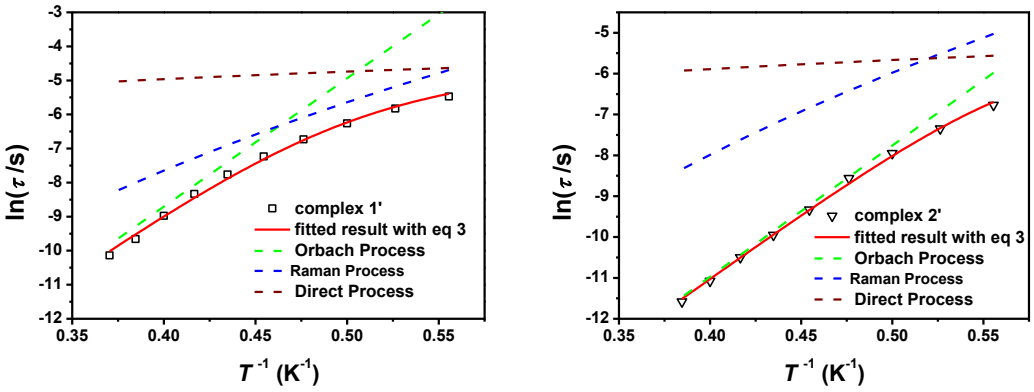

Figure S18 Arrhenius plot of ln τ as a function of T^{-1}. Open symbols are points derived from experimental data for the slow relaxation process. Dashed lines are the different contributions to the slow relaxation process: Wine = direct, Green = Orbach, Blue = Raman. The solid line is the sum of these contributions.

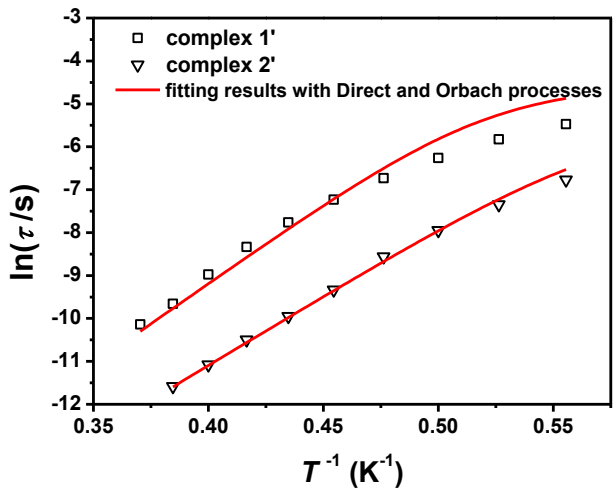

Figure S19 Temperature dependence of ln(τ) extracted from ac susceptibility measurements for complexes **1'** and **2'** at different temperatures. The solid lines are fitting results with $\tau^{-1} = A_1H^4T + A_2H^2T + \tau_0^{-1}\exp(-\frac{U}{k_BT})$.

Table S6. Analysis of Cole-Cole plot of complex **2'** under 600 Oe dc field

T/ K	χ_S(cm^{3}mol^{-1})	χ_t (cm^{3}mol^{-1})	τ (s)	α	*R*
1.8	0.910	5.99	1.15E-03	7.41E-02	8.14E-02
1.9	0.891	5.71	6.44E-04	5.34E-02	6.00E-02
2.0	0.877	5.45	3.53E-04	4.21E-02	1.06E-01
2.1	0.992	5.17	2.01E-04	5.88E-03	1.41E-01
2.2	0	5.01	8.00E-05	7.51E-02	8.13E-02
2.3	0	4.81	4.76E-05	2.75E-02	2.26E-02
2.4	1.21E-11	4.62E+00	2.75E-05	1.04E-15	5.53E-02
2.5	1.86E-11	4.46E+00	1.55E-05	1.15E-15	8.14E-02
2.6	2.48E-11	4.33E+00	9.32E-06	1.27E-15	4.56E-02
2.7	3.43E-11	4.18E+00	4.77E-06	1.69E-15	5.32E-02
2.8	5.81E-11	4.05E+00	2.78E-06	1.68E-15	8.63E-02
2.9	8.78E-11	3.94E+00	9.01E-07	2.41E-15	8.03E-02
3.0	1.98E-10	3.82E+00	9.60E-20	3.52E-15	5.15E-02
3.1	1.77E-10	3.72E+00	9.73E-20	4.26E-15	4.40E-02

3. Theoretical calculation

Table S7. The ***g*** (g_x, g_y, g_z) tensors of the lowest Kramers doublets (KDs) of the Er(III) fragments of complexes **1**–**2**.

KDs		1		2	
		g	**E(cm^{-1})**	**g**	**E(cm^{-1})**
1	g_x	9.800	0.0	10.057	0.0
	g_y	6.404		5.535	
	g_z	0.971		0.228	
2	g_x	0.170	19.3	9.576	15.3
	g_y	4.179		5.845	
	g_z	12.515		0.058	
3	g_x	0.461	40.0	1.815	39.7
	g_y	2.381		3.196	
	g_z	9.644		8.999	
4	g_x	1.802	73.2	0.082	79.5
	g_y	2.821		3.409	
	g_z	7.305		7.681	
5	g_x	2.454	115.1	1.979	111.9
	g_y	5.232		4.581	
	g_z	8.515		9.080	
6	g_x	0.418	155.6	0.118	153.6
	g_y	2.139		2.785	
	g_z	12.247		11.733	
7	g_x	6.784	200.7	4.507	196.4
	g_y	6.200		4.894	
	g_z	5.069		8.500	
8	g_x	0.542	258.3	0.333	266.3
	g_y	1.066		0.625	
	g_z	15.914		16.359	

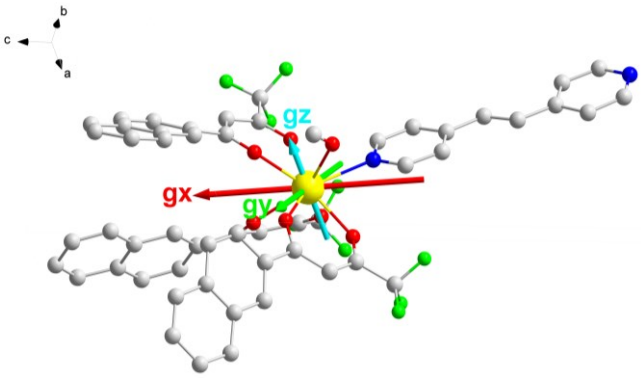

1

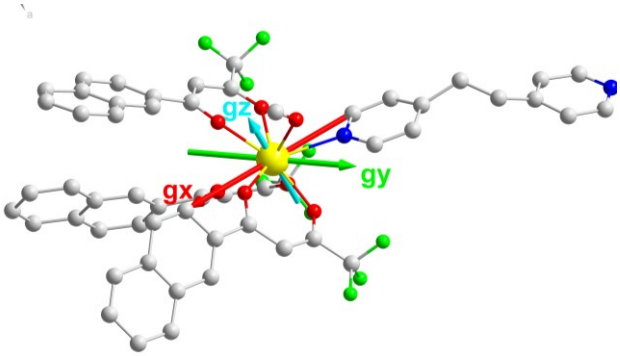

2

Figure S20. Orientations of the local main magnetic axes of the ground Kramers doublet on Er(III) of complexes **1** and **2**.

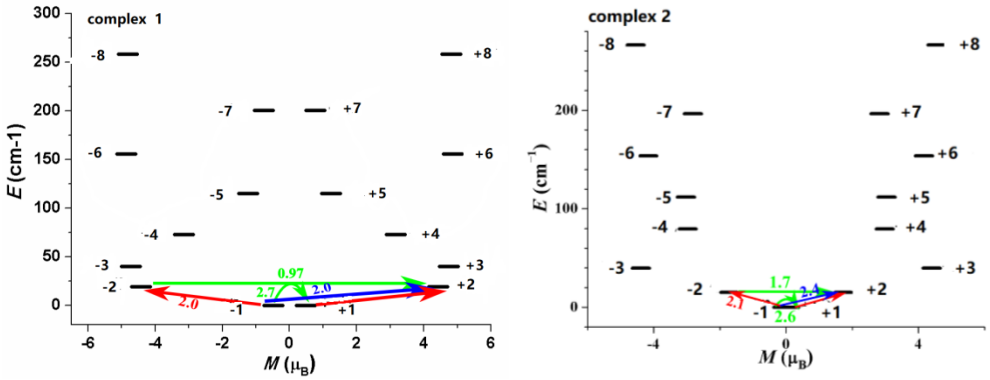

Figure S21. Magnetization blocking barriers in **1** and **2**. The thick black lines represent the Kramers doublets as a function of their magnetic moment along the magnetic axis. The green lines correspond to diagonal quantum tunnelling of the magnetization (QTM); the blue line represents off-diagonal relaxation process. The numbers at each arrow refer to the mean absolute value of the corresponding matrix element of transition magnetic moment.

4. Reference

(S1) (a) Madison, W. SAINT v5.0–6.01, Bruker Analytical X-ray Systems Inc, 1998. (b) Sheldrick, G. M. SADABSs: *An Empirical Absorption Correction Program*, **1996**. (c) Patterson, A. L. *Phys*. *Rev*. **1934**, *46*, 372. (d) SHELXTL 6.10, Bruker Analytical Instrumentation: Madison, WI, **2000.**

(S2) Alvarez, S.; Avnir, D.; Llunell, M.; Pinsky, M. Continuous symmetry maps and shape classification. The case of six-coordinated metal compoundsElectronic supplementary information (ESI) available: tables of CSD refcodes, structural parameters and symmetry measures for the studied compounds. *New J. Chem*. **2002**, *26*, 996-1009.